

SUPPLEMENTARY MATERIAL

The automation of robust interatomic-force measurements

John Elie Sader*

*ARC Centre of Excellence in Exciton Science, School of Mathematics and Statistics, The University of Melbourne,
Victoria 3010, Australia*

*Email: jsader@unimelb.edu.au

1. User guide: automated software

Software, in the form of a Mathematica notebook, is provided that automates the inflection point test [1] algorithm in Fig. 1 (dashed box) together with the Sader-Jarvis method [2] for force recovery. Here, we demonstrate the operation of this software and provide guidance for its practical use. Basic inputs are required under the following headings:

- i. **INPUT - Oscillation amplitude (m)**. The oscillation amplitude used to measured the frequency shift vs distance data.
- ii. **INPUT - Cantilever spring constant (N/m)**. The cantilever's dynamic spring constant.
- iii. **INPUT - Resonant frequency far from surface (Hz)**. The resonant frequency of the cantilever in the absence of an interaction force.
- iv. **INPUT - Frequency shift (Hz) vs distance (m) data file**. The measured frequency shift versus distance data file with two (tab delimited or space separated) columns: distance (m) & frequency shift (Hz).

The software automatically recovers the force using the Sader-Jarvis method and applies the inflection point test, returning:

- i. **OUTPUT**. The original frequency shift data, recovered force (figure and CSV file in the current directory), an assessment of its validity and a guide to amplitudes for valid force measurements.

EXAMPLE IMPLEMENTATIONS

We study two model force curves: one force curve gives valid and robust force recovery for all amplitudes, while the other can produce ill-posed results. The real experimental situation is simulated by:

1. determining the frequency shift versus distance curve (using Eq. (1)); and
2. recovering the force from this frequency-distance data using the Sader-Jarvis method and assessing its validity using the inflection point test, as embodied in the software.

This two-step process mimics the measurement process (see text).

Matrix method. To demonstrate that the inflection point test automation reported in this study can be used with any force recovery method—provided it is formulated for arbitrary amplitude—we also apply it to the recovered force obtained using the matrix method. The matrix method is implemented using separate in-house code and bypassing the Sader-Jarvis code in the software.

A. Exponentially decaying force-distance curve

The first force law considered decays exponentially with distance, z , and contains no inflection points,

$$F(z) = F_0 \exp\left(-\frac{z}{\lambda}\right), \quad z \geq 0, \quad (\text{S1})$$

where F_0 is the maximal force and λ is the length scale of the decay. Here, we choose $\lambda = 1 \text{ \AA}$ and $F_0 = 1 \text{ nN}$.

AFM operating conditions. We use the following cantilever properties: dynamic spring constant, $k = 2,000 \text{ N/m}$, and resonant frequency, $f_0 = 20,000 \text{ Hz}$. The oscillation amplitude is set to $a = 1.5 \text{ \AA}$, and thus comparable to the length scale of the force, λ ; this is precisely where ill-posed behavior can emerge, if it exists [1]. Uncertainty in measuring the oscillation amplitude always arises in a real experiment. This is modeled by overestimating the true amplitude by +10% when performing the force recovery, as used in Ref. 1; this uncertainty margin is not atypical in practice.

Simulated FM-AFM force measurement

Step 1. The required frequency-distance data file is generated by substituting Eq. (S1) into Eq. (1) and discretizing the result over the spatial interval $0 \leq z \leq 10 \text{ \AA}$; 200 data points are used here, which is typical of real FM-AFM experimental literature data.

Step 2. The resulting frequency-distance data is shown in Fig. **S1(a)** together with the resulting recovered force obtained using both the Sader-Jarvis and matrix methods. For comparison, the true force is also shown in red where it is clear that both methods work well: the recovered and true forces agree. In a real experiment, this latter comparison cannot be made—here, it aids in identifying the presence of ill-posed behavior (none is observed) and is used to assess the software output.

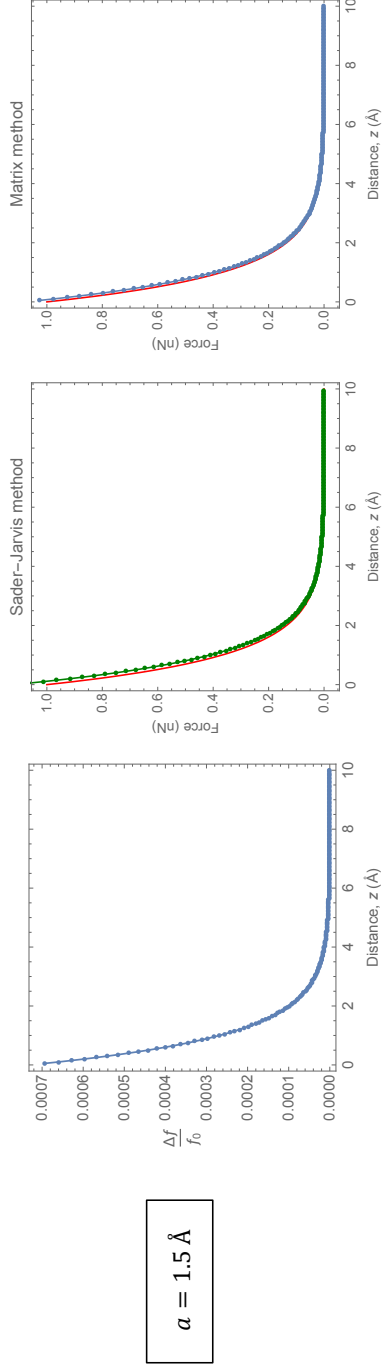
Step 3. The software then produces the outputs in Fig. **S1(b)**, which show the frequency shift, recovered force and an assessment of its validity.

The software reports that the recovered force curves obtained using both the Sader-Jarvis and matrix methods are valid for any oscillation amplitude. This is expected because the force law in Eq. (S1) contains no inflection points [1]. It is also consistent with comparisons to the true force law in Fig. **S1(a)**.

Using different oscillation amplitudes gives similar valid recovered force curves (not shown)—because there is no forbidden zone—which establishes that any of these recovered force curves constitute a robust force ‘measurement’.

This example demonstrates the utility of the software in identifying valid force recovery on discrete force-distance data, i.e., the real experimental situation, and establishing a robust force measurement.

(a) Frequency and recovered force-distance curves



(b) OUTPUT: Mathematica notebook

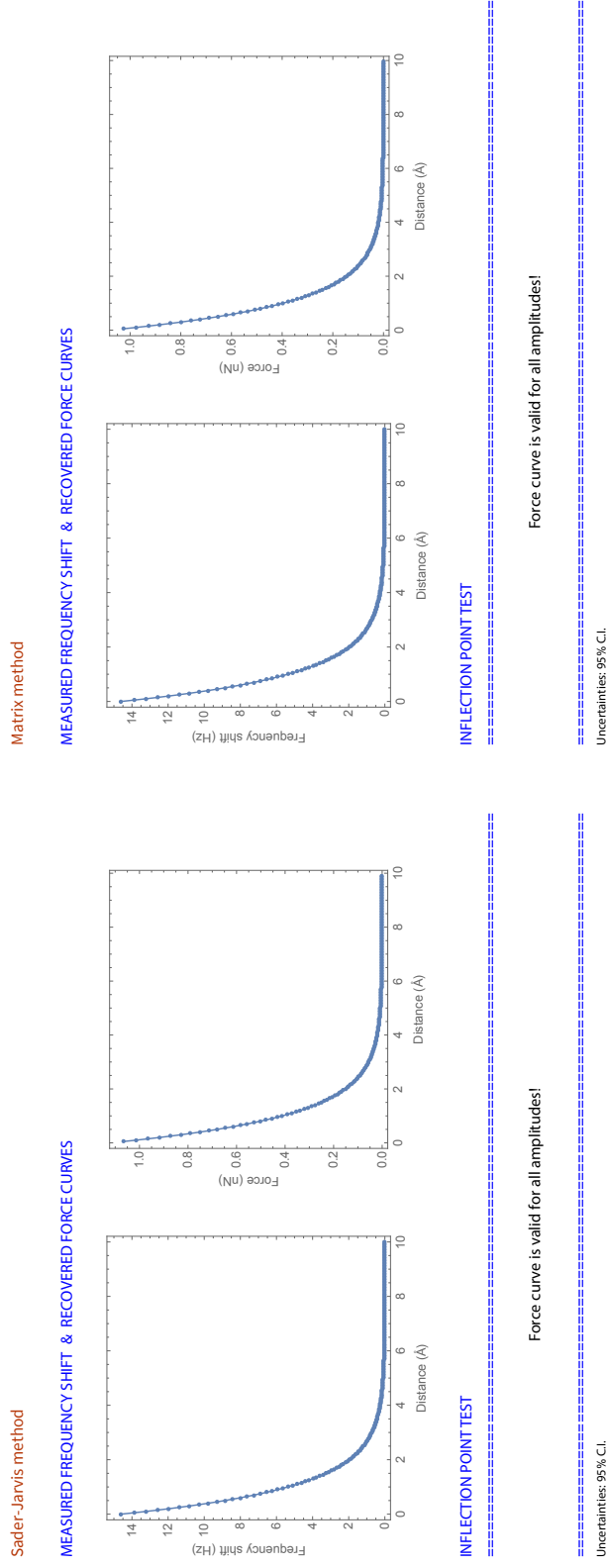


FIG. S1: Exponentially decaying force-distance law. Simulated FM-AFM force measurement and application of the inflection point test. (a) Simulated frequency shift and recovered force curves. (b) Output of automated software.

B. Oscillatory and decaying force-distance law

The second force-distance law exhibits spatial oscillations, decays with distance and contains an infinite number of inflection points,

$$F(z) = F_0 \exp\left(-\frac{z}{\lambda}\right) \cos\left(\frac{2\pi z}{T}\right), \quad (\text{S2})$$

where λ is length scale over which the force decays while T is its periodic length scale. This force law mimics the short-range forces induced by structural ordering of liquid molecules near a solid interface [3, 4]. It also does not belong to Laplace space, i.e., its inverse Laplace transform does not exist, indicating its FM-AFM force measurement can be ill-posed [1].

Analytical inflection point test. The inflection point test [1] is applied analytically to Eq. (S2) and yields the following forbidden zone (where ill-posed behavior can exist),

$$\left(\frac{4\pi^2}{T^2} + \frac{1}{\lambda^2}\right)^{-\frac{1}{2}} \lesssim a \lesssim z_{\text{inf}}^{(n)}, \quad (\text{S3})$$

for each inflection point,

$$z_{\text{inf}}^{(n)} = \frac{T}{2} \left[n + \frac{1}{\pi} \tan^{-1}\left(\frac{\pi\lambda}{T} - \frac{T}{4\pi\lambda}\right) \right], \quad n = 0, 1, 2, \dots \quad (\text{S4})$$

Note that the lower limit of Eq. (S3) is independent of the inflection point index, n .

Here, we choose $F_0 = 10$ nN and $\lambda = T = 3$ Å, length scales which are motivated by reported measurements of water [3, 4]. Equations (S3) and (S4) then give the following analytical expressions for the individual forbidden zones,

$$0.472 \lesssim a \lesssim \frac{z_{\text{inf}}^{(n)}}{2} \text{ (Å)}, \quad (\text{S5})$$

where the inflection points are

$$z_{\text{inf}}^{(n)} \approx 0.599 + 1.5n \text{ (Å)}, \quad n = 0, 1, 2, \dots \quad (\text{S6})$$

AFM operating conditions. These are identical to those used for the exponentially decaying force in Section 1-A. The chosen oscillation amplitude of $a = 1.5$ Å is comparable to both length scales, $\lambda = T = 3$ Å, of the force law in Eq. (S2), which again is precisely where ill-posed behavior can occur. Indeed, analytical solution to the inflection point test in Eq. (S5) shows that the measurement can exhibit ill-posed behavior for this chosen amplitude of $a = 1.5$ Å. Equation (S5) is used to benchmark the software.

Simulated FM-AFM force measurement 1 ($a = 1.5$ Å)

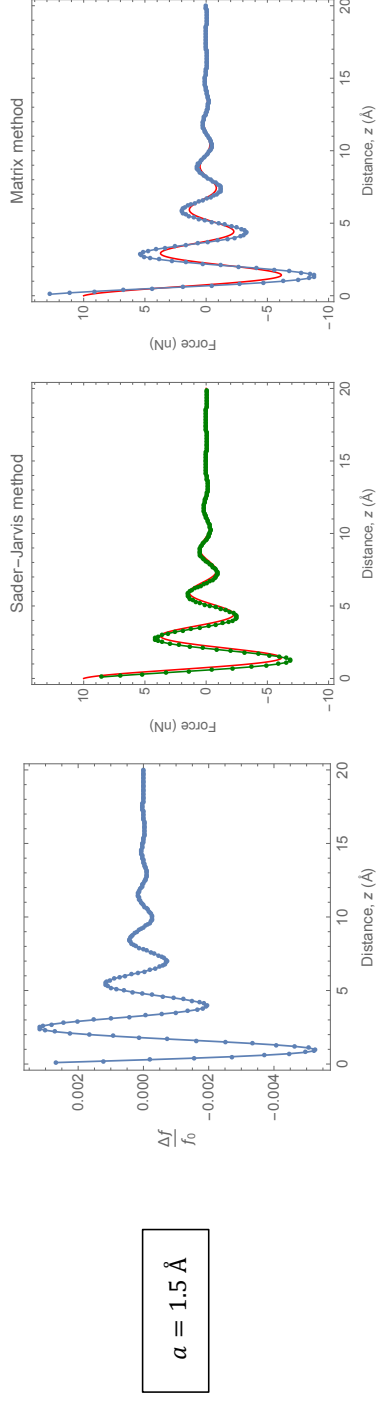
Step 1. The required frequency-distance data file is generated by substituting Eq. (S2) into Eq. (1) and discretizing the result over the spatial interval $0 \leq z \leq 20$ Å; again, 200 spatial data points are used.

Step 2. The resulting frequency-distance data is shown in Fig. **S2(a)** together with the recovered force obtained using the Sader-Jarvis and matrix methods, with a ‘measurement’ amplitude of $a = a_{\text{new}} = 1.1 \times 1.5 = 1.65$ Å (simulating experimental uncertainty). These methods give different recovered force-distance curves, with the matrix method exhibiting greater discrepancy (relative to the true force law)—this exceeds known inversion errors in these methods. The Sader-Jarvis method produces a recovered force closely aligned with the true force.

Step 3. The software then produces the outputs in Fig. **S2(b)**.

The software advises that the recovered force (obtained using both Sader-Jarvis and matrix methods) is ill-posed for the chosen oscillation amplitude of $a = 1.1 \times 1.5 = 1.61$ Å. Note that the maximal forbidden zone in Fig. **S2(b)** agrees with the analytical solution for the individual forbidden zones in Eq. (S5), while being generated purely from

(a) Frequency and recovered force-distance curves



(b) OUTPUT: Mathematica notebook

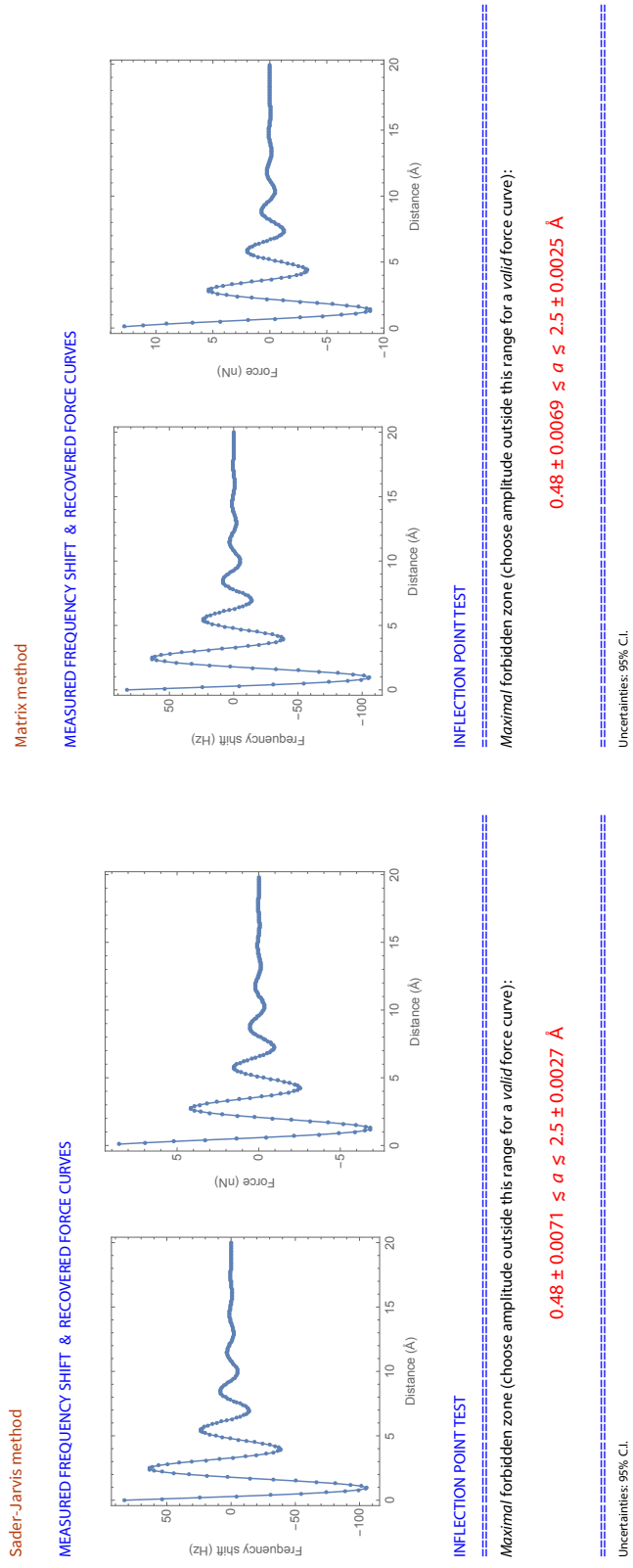


FIG. S2: Oscillatory and decaying force-distance law. Simulated FM-AFM force measurement and application of the inflection point test using $a = 1.5 \text{ \AA}$ (with +10% amplitude uncertainty for force recovery). (a) Simulated frequency shift and recovered force curves. (b) Output of automated software. Uncertainties are 95% C.I. from fits to Eq. (7) only.

discrete numerical data [5]. The observed large discrepancy in the output of the matrix method relative to the true force (in Fig. **S2(a)**) is consistent with this observation.

Comparison of Eq. (S5) and Fig. **S2(b)** demonstrates the efficacy of the software in automatically implementing the inflection point test on discrete force curves, as needed by AFM practitioners. The software guides the practitioner to choose a new amplitude, a_{new} , outside of the maximal forbidden zone,

$$0.48 \lesssim a \lesssim 2.5 \text{ (\AA)}, \quad (\text{S7})$$

which agrees well with the analytical solution in Eq. (S5). The upper limit chosen by the notebook in Eq. (S7) ensures (i) the necessary and sufficient condition, Eq. (4), is implemented and (ii) the inflection point does not occur in the measurement noise floor at large distance [5].

Important. The observed agreement between the true force and the force law generated by the Sader-Jarvis method (Fig. **S2(a)**(middle)), with the matrix method providing an erroneous result (Fig. **S2(a)**(right)), does not suggest that the Sader-Jarvis method should be used in the forbidden zone. Instead, it highlights that such an erroneous conclusion must be avoided. Neither the Sader-Jarvis or matrix method should be used in the forbidden zone, because they are not designed to handle the ill-posedness that can exist there. This provides a counterexample to Fig. 3(b).

Guided by the advice from the software, we choose a new oscillation amplitude, $a = a_{\text{new}} = 5 \text{ \AA}$ —above the upper limit of Eq. (S7)—and repeat the FM-AFM force measurement. This is discussed in ‘Simulated FM-AFM force measurement 2 ($a = 5 \text{ \AA}$)’ below. Because the upper limit of Eq. (S7) is approximate, choosing a new amplitude well above the upper limit is advisable.

Simulated FM-AFM force measurement 2 ($a = 5 \text{ \AA}$)

Step 1. The newly chosen oscillation amplitude of $a = a_{\text{new}} = 5 \text{ \AA}$ is used and the required frequency-distance data file is generated, as before.

Step 2. This frequency-distance data is shown in Fig. **S3(a)** together with the resulting recovered force obtained using the Sader-Jarvis and matrix methods, with a ‘measurement’ amplitude of $a = a_{\text{new}} = 1.1 \times 5 = 5.5 \text{ \AA}$ (simulating experimental uncertainty). Both methods now give good agreement with the true force curve.

Step 3. The software then produces the outputs in Fig. **S3(b)**.

The software now advises that the recovered forces from the Sader-Jarvis and matrix methods using the amplitude of $a = 5.5 \text{ \AA}$ are valid; see Fig. **S3(b)**. Note that this new amplitude of $a = 5.5 \text{ \AA}$ is outside of all individual forbidden zones in Fig. **S3(b)**. The individual forbidden zones for each inflection point may not necessarily overlap; they guide the practitioner to additional amplitudes where the force recovery is valid. In line with the assessment that the recovered force is valid, the Sader-Jarvis and matrix methods produce force laws that overlap with the true force.

As discussed in the text and Ref. 1, it is always important to perform force measurements using multiple amplitudes outside the forbidden zone—to show independence of valid force measurements on the chosen oscillation amplitude—and hence establish a robust force measurement. Accordingly, we conduct a further simulated measurement but now using an oscillation amplitude below the lower limit of all forbidden zones in Fig. **S3(b)**: $a = a_{\text{new}} = 0.1 \text{ \AA}$, which is again well away from the approximate lower limit. Details are discussed next in ‘Simulated FM-AFM force measurement 3 ($a = 0.1 \text{ \AA}$)’.

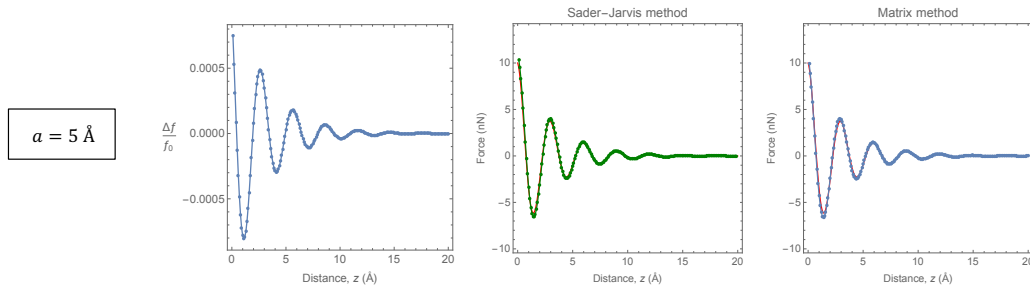
Simulated FM-AFM force measurement 3 ($a = 0.1 \text{ \AA}$)

Step 1. The additional chosen oscillation amplitude of $a = a_{\text{new}} = 0.1 \text{ \AA}$ is used and the required frequency-distance data file generated again.

Step 2. This frequency-distance data is shown in Fig. **S4(a)** together with the recovered force obtained using the Sader-Jarvis and matrix methods, with a ‘measurement’ amplitude of $a = a_{\text{new}} = 1.1 \times 0.1 = 0.11 \text{ \AA}$ (simulating experimental uncertainty). Both methods again give good agreement with the true force curve.

Step 3. The software then produces the outputs in Fig. **S4(b)**.

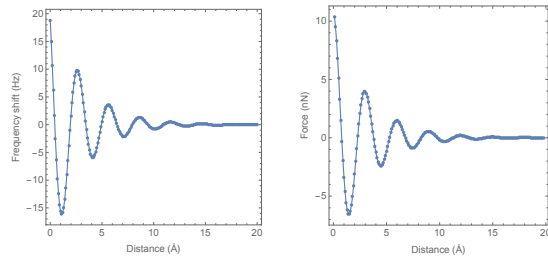
(a) Frequency and recovered force-distance curves



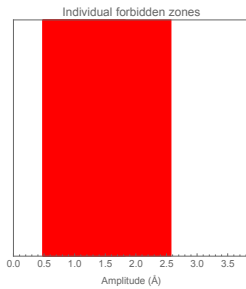
(b) OUTPUT: Mathematica notebook

Sader-Jarvis method

MEASURED FREQUENCY SHIFT & RECOVERED FORCE CURVES



INFLECTION POINT TEST

Valid force measurement: chosen amplitude, $a = 5.5 \text{ \AA}$, is outside of maximal forbidden zone.

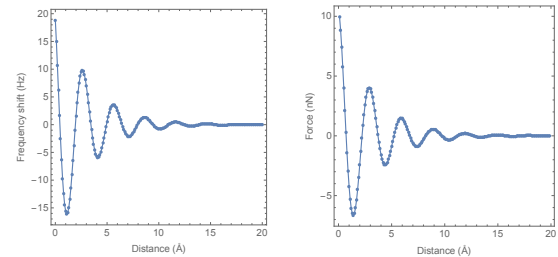
Individual forbidden zones (from each inflection point):

1. $0.49 \pm 0.0071 \leq a \leq 1.1 \pm 0.0013 \text{ \AA}$
2. $0.48 \pm 0.0067 \leq a \leq 1.8 \pm 0.0013 \text{ \AA}$
3. $0.49 \pm 0.012 \leq a \leq 2.6 \pm 0.0024 \text{ \AA}$

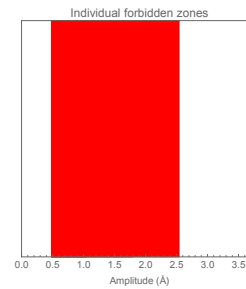
Uncertainties: 95% C.I.

Matrix method

MEASURED FREQUENCY SHIFT & RECOVERED FORCE CURVES



INFLECTION POINT TEST

Valid force measurement: chosen amplitude, $a = 5.5 \text{ \AA}$, is outside of maximal forbidden zone.

Individual forbidden zones (from each inflection point):

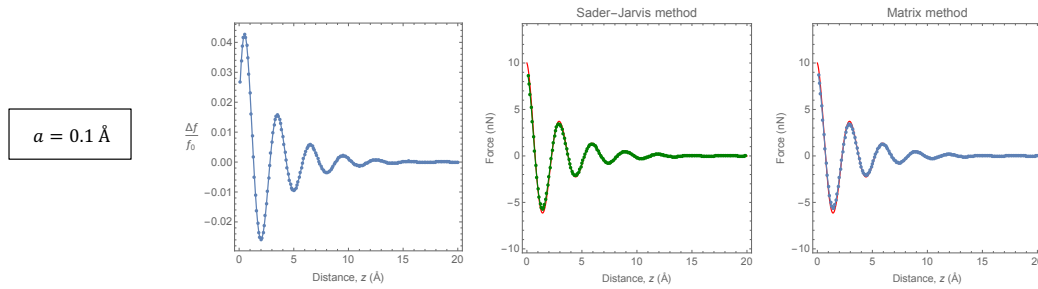
1. $0.48 \pm 0.0054 \leq a \leq 1.0 \pm 0.0012 \text{ \AA}$
2. $0.49 \pm 0.010 \leq a \leq 1.8 \pm 0.0018 \text{ \AA}$
3. $0.48 \pm 0.010 \leq a \leq 2.5 \pm 0.0018 \text{ \AA}$

Uncertainties: 95% C.I.

FIG. S3: Oscillatory and decaying force-distance law. Simulated FM-AFM force measurement and application of the inflection point test using $a = 5 \text{ \AA}$ (with +10% amplitude uncertainty for force recovery). (a) Simulated frequency shift and recovered force curves. (b) Output of automated software. Uncertainties are 95% C.I. from fits to Eq. (7) only.

The software again advises that the recovered force is valid and reports individual forbidden zones in Fig. S4(b) that are identical to those in Fig. S3(b) (obtained using a different amplitude). This is expected because the recovered force is valid in both cases and thus should be independent of the chosen measurement amplitude. The recovered forces obtained using the Sader-Jarvis and matrix methods again agree well with the true force, see Fig. S4(a), consistent with the software output.

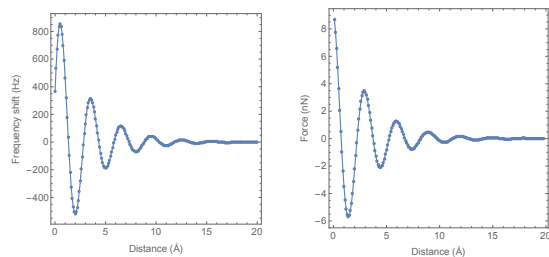
(a) Frequency and deconvoluted force-distance curves



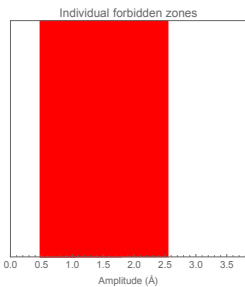
(b) OUTPUT: Mathematica notebook

Sader-Jarvis method

MEASURED FREQUENCY SHIFT & RECOVERED FORCE CURVES



INFLECTION POINT TEST

Valid force measurement: chosen amplitude, $a = 0.11 \text{ \AA}$, is outside of maximal forbidden zone.

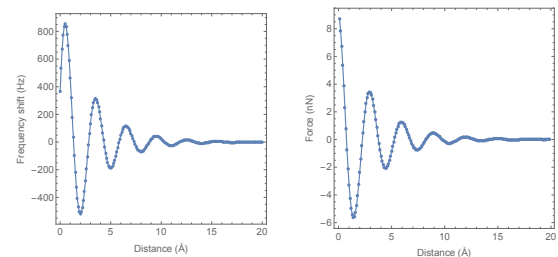
Individual forbidden zones (from each inflection point):

1. $0.48 \pm 0.0047 \leq a \leq 1.0 \pm 0.0011 \text{ \AA}$
2. $0.49 \pm 0.0094 \leq a \leq 1.8 \pm 0.0016 \text{ \AA}$
3. $0.48 \pm 0.0092 \leq a \leq 2.5 \pm 0.0016 \text{ \AA}$

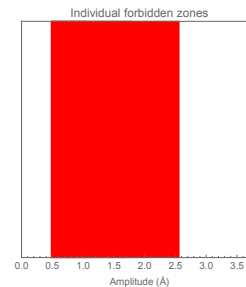
Uncertainties: 95% C.I.

Matrix method

MEASURED FREQUENCY SHIFT & RECOVERED FORCE CURVES



INFLECTION POINT TEST

Valid force measurement: chosen amplitude, $a = 0.11 \text{ \AA}$, is outside of maximal forbidden zone.

Individual forbidden zones (from each inflection point):

1. $0.48 \pm 0.0040 \leq a \leq 1.1 \pm 0.0010 \text{ \AA}$
2. $0.49 \pm 0.0092 \leq a \leq 1.8 \pm 0.0019 \text{ \AA}$
3. $0.49 \pm 0.0090 \leq a \leq 2.6 \pm 0.0019 \text{ \AA}$

Uncertainties: 95% C.I.

FIG. S4: Oscillatory and decaying force-distance law. Simulated FM-AFM force measurement and application of the inflection point test using $a = 0.1 \text{ \AA}$ (with +10% amplitude uncertainty for force recovery). (a) Simulated frequency shift and recovered force curves. (b) Output of automated software. Uncertainties are 95% C.I. from fits to Eq. (7) only.

Robust force measurement

Because two valid recovered force curves that use different oscillation amplitudes ($a = 0.1 \text{ \AA}$ and $a = 5 \text{ \AA}$) agree, we can conclude that a robust force curve has been ‘measured’; see text. This is also obvious here by comparison to the true force, which is not available in a real measurement.

In practice, use of more than two amplitudes outside the forbidden zone may be preferable.

2. Sample fits to Eq. (7) from the automated software

The software is fully automated. It first recovers the force using the Sader-Jarvis method, then fits Eq. (7) to this discrete force data to determine the inflection points and force derivatives at these points, thereby evaluating the S -factor at each inflection point. This information is substituted into Eq. (5) to identify the forbidden zones. Figures **S5** and **S6** show sample fits to Eq. (7) and S -factors for force-distance curves in Fig. 3; the force curves are identical to those reported in Ref. 6, as discussed in the text. While the z -ranges—over which fits to Eq. (7) occur—differ for the Sader-Jarvis and matrix methods, the resulting S -factors are consistent. These z -ranges are automatically determined by the software and do not require user input. The outputs in Figs. **S5** and **S6** are hidden by default in the software, and can be displayed by changing the `showintermediatesteps` variable; see `INPUT` → Other operating parameters (advanced users only).

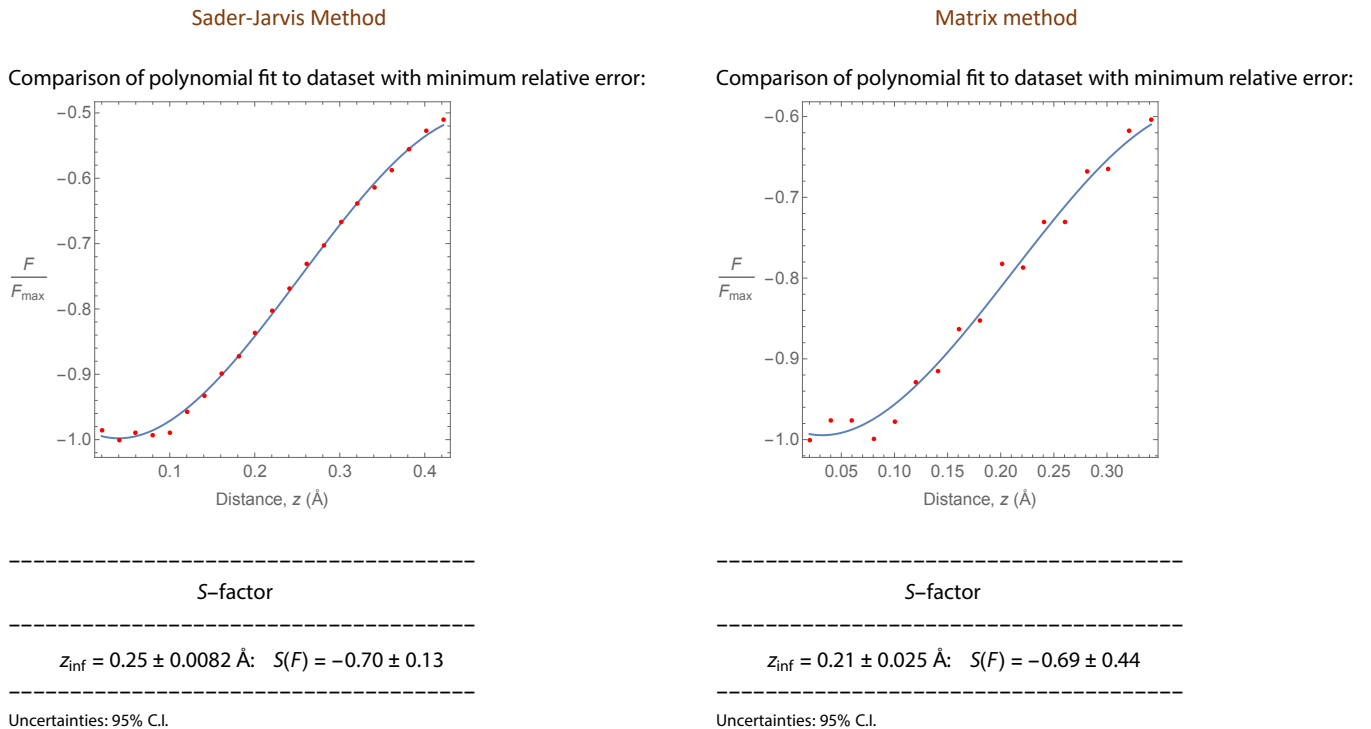
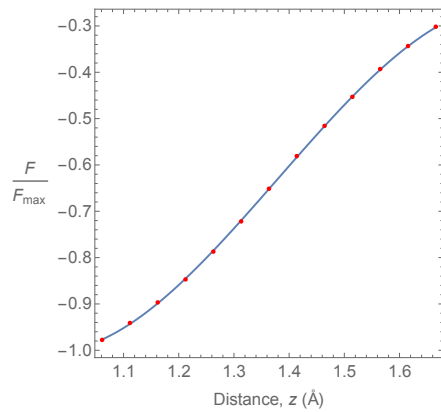


FIG. S5: CO/Cu(111) dataset using $a = 75 \text{ pm}$. Sample fits of Eq. (7) to two force-distance curves in Fig. 3(a) (obtained using Sader-Jarvis and matrix methods), generated by the automated software. Sader-Jarvis method: Two other inflection points are identified, but one does not satisfy Eq. (4) and the other has $S(F) > 0$ (no force jump). Matrix method: Recovered force has more noise than Sader-Jarvis method (see plot), leading to identification of additional inflection points; these all have $S(F) > -1$ (well-posed) with uncertainties larger than their S -factor. Both methods show that this force measurement is valid for all amplitudes because $S(F) \gtrsim -1$; see Eq. (2). Uncertainties are 95% C.I. from fits to Eq. (7) only.

Sader-Jarvis Method

Comparison of polynomial fit to dataset with minimum relative error:



S-factor

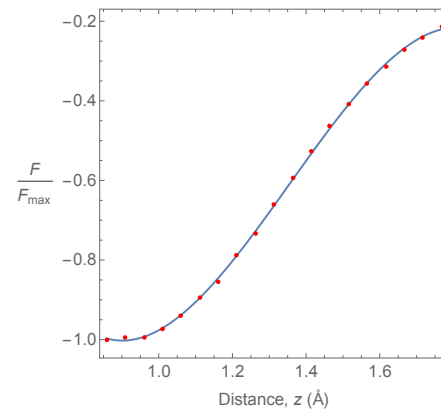
$$z_{\text{inf}} = 1.4 \pm 0.0030 \text{ \AA}; \quad S(F) = -5.7 \pm 0.31$$

$$0.29 \pm 0.0085 \lesssim a \lesssim 0.69 \pm 0.0015 \text{ \AA}$$

Uncertainties: 95% C.I.

Matrix method

Comparison of polynomial fit to dataset with minimum relative error:



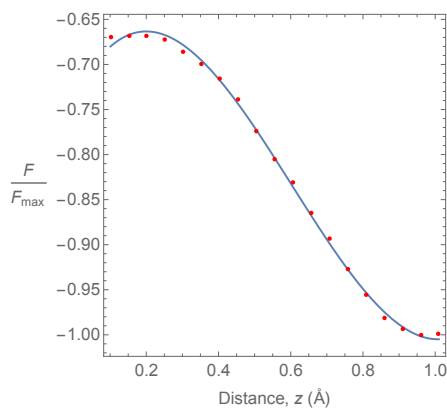
S-factor

$$z_{\text{inf}} = 1.4 \pm 0.0063 \text{ \AA}; \quad S(F) = -4.5 \pm 0.32$$

$$0.32 \pm 0.013 \lesssim a \lesssim 0.68 \pm 0.0032 \text{ \AA}$$

Uncertainties: 95% C.I.

Comparison of polynomial fit to dataset with minimum relative error:



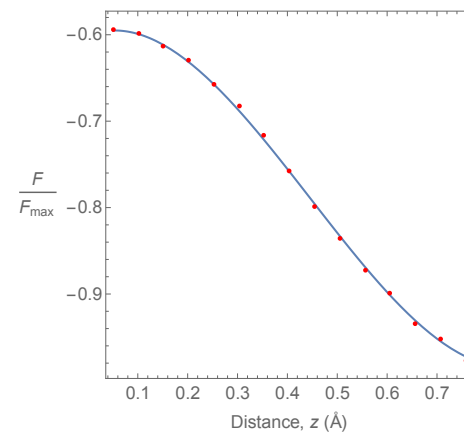
S-factor

$$z_{\text{inf}} = 0.60 \pm 0.010 \text{ \AA}; \quad S(F) = -1.1 \pm 0.14$$

$$0.29 \pm 0.023 \lesssim a \lesssim 0.30 \pm 0.0052 \text{ \AA}$$

Uncertainties: 95% C.I.

Comparison of polynomial fit to dataset with minimum relative error:



S-factor

$$z_{\text{inf}} = 0.45 \pm 0.010 \text{ \AA}; \quad S(F) = -0.64 \pm 0.091$$

Uncertainties: 95% C.I.

FIG. S6: Fe trimer/Cu(111) dataset with $a = 30$ pm. Sample fits of Eq. (7) to two force-distance curves in Fig. 3(b) (obtained using the Sader-Jarvis and matrix methods), generated by the automated software. The amplitude used for this force measurement is on the lower edge of the maximal forbidden zones: Sader-Jarvis method, $0.29 \pm 0.023 \lesssim a \lesssim 0.69 \pm 0.0015$ Å; Matrix method, $0.32 \pm 0.013 \lesssim a \lesssim 0.68 \pm 0.0032$ Å. Such borderline measurements should be avoided, with the amplitude chosen to be well outside of the forbidden zone; see text. Uncertainties are 95% C.I. from fits to Eq. (7) only.

3. Fit data generated by the automated software

Tables **S1** and **S2** lists all fit parameters automatically generated by the software for the recovered experimental force-distance curves in Figs. 3 and 5, respectively. This collective dataset illustrates how the maximal forbidden zone is derived from the individual forbidden zones of each inflection point.

Force measurement dataset	Deconvolution method	Amplitude (pm)	z_{inf} (Å)	S-factor	Individual forbidden zone (Å)	Maximal forbidden zone (Å)	Valid force curve	
CO/Cu(111)	Sader-Jarvis	100	0.28 ± 0.0093	-0.81 ± 0.15	-	-	Y	
		75	0.25 ± 0.0082	-0.70 ± 0.13	-	-	Y	
		50	0.27 ± 0.0047	-0.79 ± 0.079	-	-	Y	
		30	0.30 ± 0.0063	-0.81 ± 0.095	-	-	Y	
	Matrix	100	0.28 ± 0.0048	-0.78 ± 0.077	-	-	Y	
		75	0.27 ± 0.016	-0.77 ± 0.27	-	-	Y	
		50	0.21 ± 0.025	-0.69 ± 0.44	-	-	Y	
		30	0.25 ± 0.014	-0.87 ± 0.28	-	-	Y	
	Fe trimer/Cu(111)	Sader-Jarvis	100	0.30 ± 0.014	-0.77 ± 0.21	-	-	Y
			75	0.26 ± 0.017	-0.68 ± 0.24	-	-	Y
			50	0.42 ± 0.031	-0.41 ± 0.16	$0.35 \pm 0.015 \lesssim a \lesssim 0.69 \pm 0.0034$	$0.35 \pm 0.015 \lesssim a \lesssim 0.69 \pm 0.0034$	Y
			30	1.4 ± 0.0067	-3.9 ± 0.30	$0.35 \pm 0.015 \lesssim a \lesssim 0.69 \pm 0.0034$	$0.35 \pm 0.015 \lesssim a \lesssim 0.69 \pm 0.0034$	Y
Matrix	100	0.55 ± 0.0062	-0.93 ± 0.069	$0.34 \pm 0.015 \lesssim a \lesssim 0.71 \pm 0.0031$	$0.34 \pm 0.015 \lesssim a \lesssim 0.71 \pm 0.0031$	N		
	75	1.4 ± 0.0062	-4.4 ± 0.34	$0.29 \pm 0.023 \lesssim a \lesssim 0.30 \pm 0.0052$	$0.29 \pm 0.023 \lesssim a \lesssim 0.30 \pm 0.0052$	N		
	50	0.60 ± 0.010	-1.1 ± 0.14	$0.29 \pm 0.0085 \lesssim a \lesssim 0.69 \pm 0.0015$	$0.29 \pm 0.0085 \lesssim a \lesssim 0.69 \pm 0.0015$	N		
	30	1.4 ± 0.0030	-5.7 ± 0.31	$0.35 \pm 0.0086 \lesssim a \lesssim 0.71 \pm 0.0020$	$0.35 \pm 0.0086 \lesssim a \lesssim 0.71 \pm 0.0020$	Y		
Fe trimer/Cu(111)	Matrix	100	0.47 ± 0.0038	-0.67 ± 0.030	-	-	Y	
		75	1.4 ± 0.0040	-4.2 ± 0.18	$0.35 \pm 0.0086 \lesssim a \lesssim 0.71 \pm 0.0020$	$0.35 \pm 0.0086 \lesssim a \lesssim 0.71 \pm 0.0020$	Y	
		50	0.46 ± 0.015	-0.61 ± 0.11	$0.35 \pm 0.014 \lesssim a \lesssim 0.69 \pm 0.0037$	$0.35 \pm 0.014 \lesssim a \lesssim 0.69 \pm 0.0037$	Y	
		30	1.4 ± 0.0074	-3.9 ± 0.26	$0.35 \pm 0.014 \lesssim a \lesssim 0.69 \pm 0.0037$	$0.35 \pm 0.014 \lesssim a \lesssim 0.69 \pm 0.0037$	Y	
Fe trimer/Cu(111)	Matrix	100	0.51 ± 0.025	-0.56 ± 0.16	-	-	N	
		75	1.4 ± 0.0062	-4.2 ± 0.28	$0.34 \pm 0.013 \lesssim a \lesssim 0.70 \pm 0.0031$	$0.34 \pm 0.013 \lesssim a \lesssim 0.70 \pm 0.0031$	N	
		50	0.45 ± 0.010	-0.64 ± 0.091	$0.32 \pm 0.013 \lesssim a \lesssim 0.68 \pm 0.0032$	$0.32 \pm 0.013 \lesssim a \lesssim 0.68 \pm 0.0032$	Borderline	
		30	1.4 ± 0.0063	-4.5 ± 0.32	$0.32 \pm 0.013 \lesssim a \lesssim 0.68 \pm 0.0032$	$0.32 \pm 0.013 \lesssim a \lesssim 0.68 \pm 0.0032$	Borderline	
Fe trimer/Cu(111)	Matrix	100	0.52 ± 0.0092	-0.74 ± 0.079	-	-	Y	
		75	1.4 ± 0.0065	-4.4 ± 0.29	$0.34 \pm 0.013 \lesssim a \lesssim 0.71 \pm 0.0033$	$0.34 \pm 0.013 \lesssim a \lesssim 0.71 \pm 0.0033$	Y	

TABLE S1: Fit data from the software for Fig. 3. Fit data including inflection points that give a significant jump in the force (i.e., Eq. (4) does not hold) with S -factor uncertainties smaller than their magnitude, values of their respective S -factors, individual forbidden zones for each inflection point, maximal forbidden zones and overall assessments of recovered force validity. Uncertainties are 95% C.I. from fits to Eq. (7) only.

Force measurement dataset	Amplitude (nm)	z_{inf} (Å)	S-factor	Individual forbidden zone (Å)	Maximal forbidden zone (Å)	Valid force curve
		3.3 ± 0.0071	-2.2 ± 0.054	$1.1 \pm 0.016 \lesssim a \lesssim 1.6 \pm 0.0035$		
		6.8 ± 0.010	-7.6 ± 0.23	$1.2 \pm 0.021 \lesssim a \lesssim 3.4 \pm 0.0051$		
		10 ± 0.0067	-16 ± 0.29	$1.3 \pm 0.013 \lesssim a \lesssim 5.2 \pm 0.0034$		
OMCTS	2.0	14 ± 0.033	-36 ± 3.4	$1.2 \pm 0.058 \lesssim a \lesssim 7.1 \pm 0.016$	$0.99 \pm 0.027 \lesssim a \lesssim 13 \pm 0.0079$	Y
		17 ± 0.0095	-70 ± 2.2	$1.0 \pm 0.017 \lesssim a \lesssim 8.6 \pm 0.0047$		
		21 ± 0.016	-62 ± 2.3	$1.3 \pm 0.025 \lesssim a \lesssim 10 \pm 0.0078$		
		24 ± 0.025	-1100 ± 8.7	$1.1 \pm 0.045 \lesssim a \lesssim 12 \pm 0.013$		
		27 ± 0.016	-1800 ± 10	$0.99 \pm 0.027 \lesssim a \lesssim 13 \pm 0.0079$		

TABLE S2: Fit data from the software for Fig. 5. Details as for Table S1 with the Sader-Jarvis method used throughout. The minimum force jump threshold is set to the observed peak noise level in Fig. 5; see text.

-
- [1] J. E. Sader, B. D. Hughes, F. Huber, and F. J. Giessibl, *Nature Nanotechnology* **13**, 1088 (2018), Extended text: <http://arxiv.org/abs/1709.07571>.
 - [2] J. E. Sader and S. P. Jarvis, *Applied Physics Letters* **84**, 1801 (2004).
 - [3] T. Uchihashi, M. J. Higgins, S. Yasuda, S. P. Jarvis, S. Akita, T. Nakayama, and J. E. Sader, *Applied Physics Letters* **85**, 3575 (2004).
 - [4] M. R. Uhlig, D. Martin-Jimenez, and R. Garcia, *Nature Communications* **10**, 2606 (2019).
 - [5] To avoid the spurious results, inflection points in the measurement noise floor at large distance (less than 5% of the maximum force) are not analyzed by the Mathematica notebook.
 - [6] F. Huber and F. J. Giessibl, *Journal of Applied Physics* **127**, 184301 (2020).